Computational Analysis of the Mechanical Behaviors of Hemiarch and Total Arch Replacements

Kuo-Sheng Liu,[1] Cheng-Hung Lee,[2] Feng-Chun Tsai,[1] Guan-Heng Jhong,[3] Kuo-Chun Hung,[2] and Shih-Jung Liu[3,4]

[1]Department of Thoracic and Cardiovascular Surgery, Chang Gung Memorial Hospital, Tao-Yuan 333, Taiwan; [2]Division of Cardiology, Department of Internal Medicine, Chang Gung Memorial Hospital, Tao-Yuan 333, Taiwan; [3]Graduate Institute of Medical Mechatronics, Chang Gung University, Tao-Yuan 333, Taiwan; and [4]Biomaterials Lab, Mechanical Engineering, Chang Gung University, No. 259, Wen-Hwa 1st Road, Kwei-Shan, Tao-Yuan 333, Taiwan

Associate Editor Aleksander S. Popel oversaw the review of this article.

Abstract—Surgery for aortic dissections or aneurysms can be extended into the aortic arch by hemiarch replacement (HAR) or total arch replacement (TAR). Although cardiovascular surgeons have been performing HAR and TAR for decades, the mechanical properties of HAR and TAR are not well understood. This study investigates the mechanical behaviors and stress distributions in HAR and TAR using a hybrid fluid–structure interaction analysis that combines computational fluid dynamics and structural static analysis. Geometrical information on the aortas of 11 subjects was extracted from contrast-enhanced computed tomography (CT) scan data. The CT images were imported into medical image processing software to reconstruct 3D models of the aortas. A 3D finite element model was employed to simulate aortas that receive HAR or TAR. The deformation of the great vessels and the stress distributions at both the vessels and the aortic grafts were calculated. The numerical results revealed that the aortas following TAR exhibited a lower level of stress than those following HAR. Higher stresses may cause arterial wall injury and increase the risk of rupture. Finite element analysis of the aortas and the aortic grafts provides useful information that helps physicians better understand the potential problems that may arise after various surgical procedures.

Keywords—Aortic arch replacement, Aortic grafts, Finite element analysis, Stress distribution.

INTRODUCTION

Surgery for aortic dissections or aneurysms can be extended into the aortic arch by hemiarch replacement (HAR) or total arch replacement (TAR), which differs in the extent of aortic arch resection. In cases of HAR, the side of the arotic arch with lesser curvature is resected well beyond the level of the takeoff of the innominate artery, while the side with greater curvature remains untouched. An aortic graft is then anastomosed to the beveled edge of the aortic arch. TAR requires a more extensive arch resection to the level beyond the left subclavian artery. Revascularization of the supra-aortic branches is required. Figure 1 schematically depicts the aortic arch that has received HAR or TAR. Although cardiovascular surgeons have performed HAR and TAR for decades, their mechanical properties are poorly understood. A number of reports have shown that an extensive TAR significantly reduces the incidence of a patent false lumen; enhances aortic remodeling, and may improve long-term outcomes for patients with acute type A aortic dissection.[8,10,20–22] We assume that the favorable results of TAR relative to those of HAR can be attributed to its beneficial mechanical effect on the aorta. This study investigates the mechanical behavior of the aorta after HAR or TAR using a computational aortic model. The biomechanical behavior of the aorta has been investigated in a cadaveric aorta[1,11] and in a mock glass aortic model.[13] However, these studies have not become popular because the source of the cadaveric aorta was restricted and the best application of the mock aortic model was limited to the relevant fluid dynamics. Computational finite element analysis (FEA) of the aorta is becoming an increasingly valuable tool for the study of aortic physiology and pathophysiology. In such an analysis, a structure of complex geometry is divided into small elements where numerical simulation is more readily executed. Solutions derived

Address correspondence to Shih-Jung Liu, Biomaterials Lab, Mechanical Engineering, Chang Gung University, No. 259, Wen-Hwa 1st Road, Kwei-Shan, Tao-Yuan 333, Taiwan. Electronic mail: shihjung@mail.cgu.edu.tw
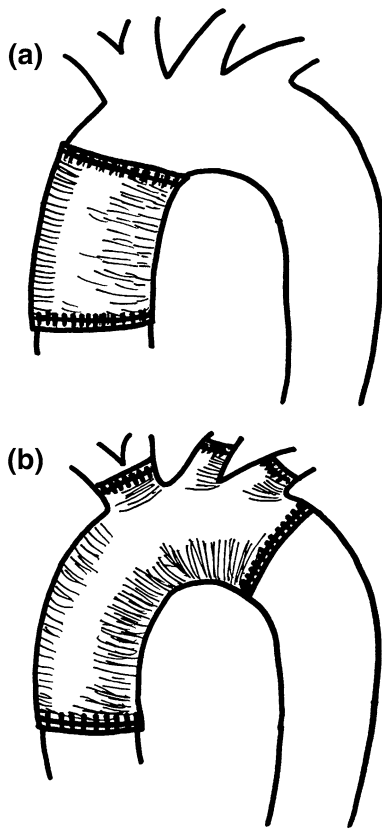
FIGURE 1. Aortic arch with (a) hemiarch replacement, (b) total arch replacement.

using these elements are subsequently reconstructed to approximate the solution for the overall structure.[17] Previous studies have focused on the pathogenesis of aortic dissection and the rupture risk stratification of abdominal and thoracic aortic aneurysms.[2,12,14,17,23] This study investigated the stress distribution in the aortic wall post-HAR and post-TAR, using a fluid–structure interaction model that combines computational fluid dynamics and structural analysis.

MATERIALS AND METHODS

The institutional review board of the Chang Gung Medical Foundation reviewed and approved the study protocol. Informed written consent was obtained from each patient before enrollment in this investigation. The study was conducted in a manner consistent with the Helsinki Declaration.

Mechanical Properties of Aortic Grafts

The tensile strengths of the Dacron vascular grafts (Hemashield Platinum, Woven Double Velour, Maquet Getinge Group, NJ, USA.) were determined.
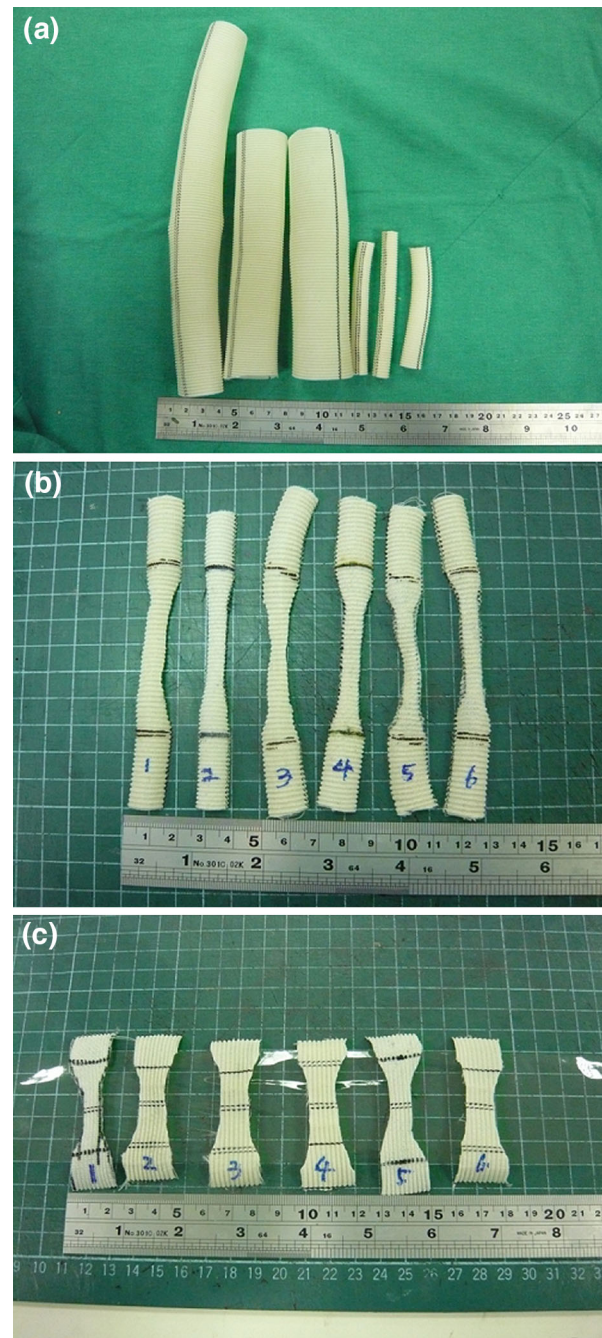

FIGURE 2. Photographs of (a) vascular grafts, and tensile test specimens in (b) axial direction and (c) circumferential direction of grafts.

The dumbbell-shaped tensile specimens with gauge lengths of 20 mm and a cross-sectional area of 6 mm wide by 0.4 mm thick were cut using a knife from the grafts in both the axial and the circumferential directions. ASTM D638 tensile tests were performed in a LLOYD tensiometer. A 500 N load cell was used and the crosshead speed was 90 mm/min. Figure 2 presents the vascular grafts and the test specimens.

Patients

Eleven patients who had undergone a computational tomography (CT) scan for the thoracic aorta were retrospectively identified from the esophageal and lung cancer database in the authors' hospital. Patients with severe aortic atherosclerotic disease, thoracic aortic aneurysms or dissections, or previous thoracic aortic operations were excluded. The study cohort ($n = 11$) consisted of eight men (73%) with an age of 58.4 ± 15.7 years (with a range of 38–86 years); their average height and weight were 1.65 ± 0.069 m (with a range of 1.50–1.74 m) and 68 ± 15 kg (with a range of 48–104 kg), respectively. All patients underwent a CT scan as a part of their preoperative tumor staging protocol, rather than for this study in particular.

Image Reconstruction

Information about the geometry of the aortas of the subjects was extracted from contrast-enhanced CT scan data. CT scans were performed using 64-slice scanners (Siemens Medical Solutions, Pennsylvania, USA) with the intravenous injection of 80–120 mL of nonionic iodinated contrast dye (Omnipaque 350, GE Amersham, Milwaukee, USA). The CT images were imported into, and analyzed using Mimics 13.0 (Materialise, Leuven, Belgium) medical image processing software: a semi-automatic segmentation algorithm was utilized to detect the aortic wall and to construct 3D models of the aortas. This algorithm used user-defined seed points and lower and upper grey-level thresholds. Figure 3 presents the results that were obtained using the segmentation algorithm.

To ensure that each slice had an accurately controlled and smooth surface, it was visually inspected. A Gaussian filter with a 3×3 kernel was used to smooth the lumen borders. For each patient, three-dimensional aortic wall surfaces were constructed from the two-dimensional contour stack and tessellated to eliminate skewed elements, which could otherwise have resulted in artificial stress concentrations. Figure 4 displays one of the solid models of a reconstructed aortic arch.

Finite Element Analysis

A fluid dynamics analysis was firstly performed to determine the pressure distribution imposed on the vessels by the blood. A finite element model of the ascending aorta, aortic arch, and supra-aortic vessels was built for stress analysis using commercial software ANSYS 13.0 (Ansys Inc., USA). As in other aortic flow studies, the blood was assumed to be homogeneous, incompressible and Newtonian, with a density of 1060 kg/m^3 and a viscosity of 0.00371 Pa s.[4,5,15,19] A no-slip condition was applied at the aortic wall. Blood flow is generally assumed to be laminar in large vessels because the mean flow velocity is low enough to result in a relatively low Reynolds number. For pulsatile unsteady flow, turbulence occurs at a Reynolds number that greatly exceeds that expected for steady flow because accelerating flow is more stable than decelerating flow.[7] In this study, only the steady state solution at the maximum flow was considered and calculated.[16] The flow pressure and velocity at the aorta inlet were assumed to be uniformly 120 mmHg (systolic blood pressure) and 0.123 m/s,[18] respectively, while the pressure that was used on the innominate artery, the left common carotid artery, the left subclavian artery and the distal aorta was 80 mmHg (diastolic blood pressure).
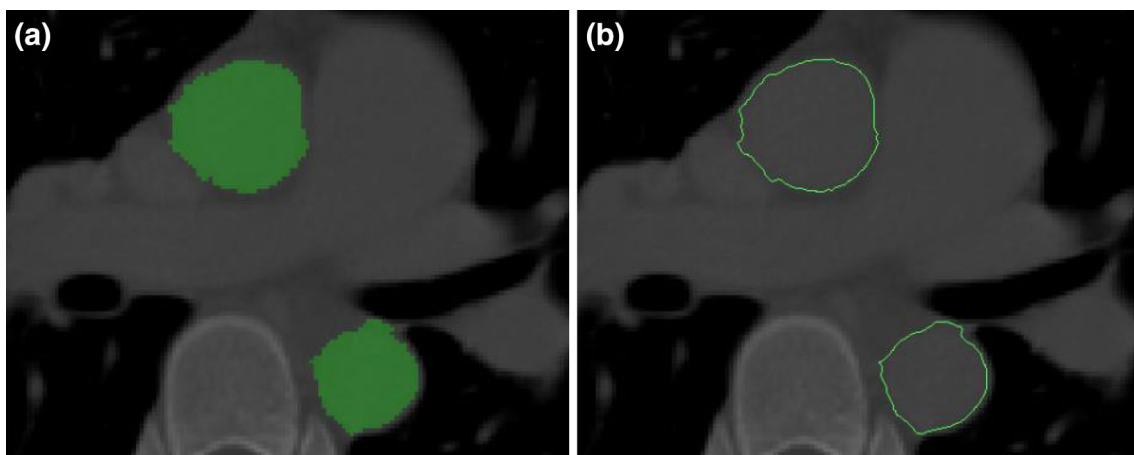

FIGURE 3. Segmentation of aorta, (a) geometry of aortas (green areas) of subjects was extracted from contrast-enhanced CT scan data, (b) CT images were imported into, and analyzed using Mimics 13.0 (Materialise, Leuven, Belgium) medical image processing software: a semi-automatic segmentation algorithm was applied to detect aortic wall (green lines) and to construct 3D models of aortas.
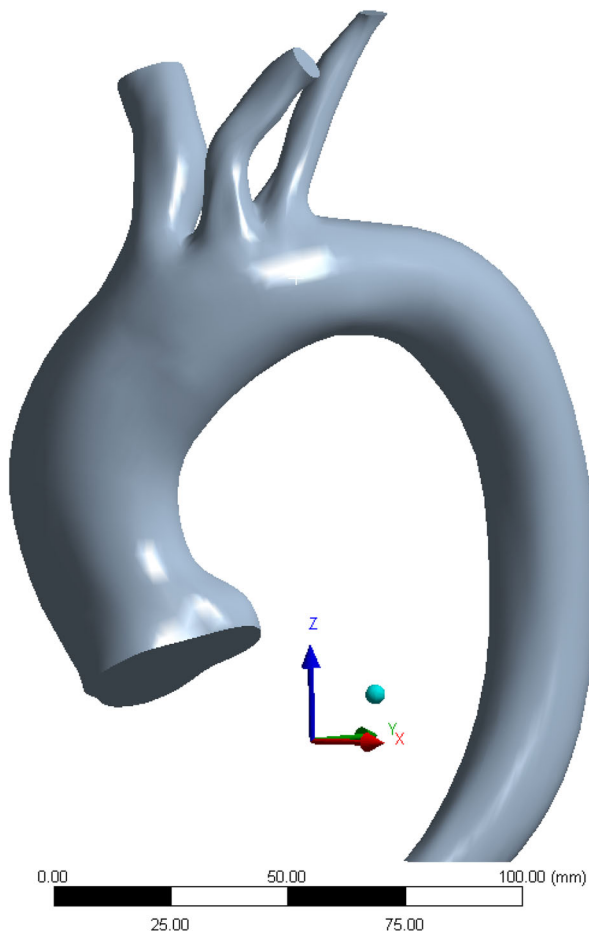
FIGURE 4. Constructed solid model of aortic artery.

FIGURE 5. Finite element mesh used in aortic model, (a) no graft, (b) following HAR, (c) following TAR.

The fluid pressure distribution that was calculated by the fluid dynamics analysis was then used as the boundary conditions for the subsequent elastic structure analysis. Again the numerical simulation was conducted using the commercial finite element package, Ansys 13.0 (Ansys Inc., USA). The aortic arch and descending thoracic aortic wall were assumed to have a uniform thickness of 2.2 mm,[3,6,9] whereas the ascending aortic wall was assumed to have a uniform thickness of 1.7 mm, based on transthoracic echocardiography data.[14] The aortic wall was assumed to be homogenous, incompressible, isotropic, and linearly elastic, with a Young's modulus of 3.0 MPa and a Poisson ratio of 0.46.[4,5,15,19] The values of the vascular graft parameters were determined from the experimental data in the tensile tests.

A semi-automatic adaptive meshing approach was utilized in Hyper Mesh 10.0 (Altair Hyper Works, Troy, MI, USA) to determine the number of elements to optimize the computational efficiency and element quality. Once the adequate boundary conditions were applied to each model, a mesh was generated on each
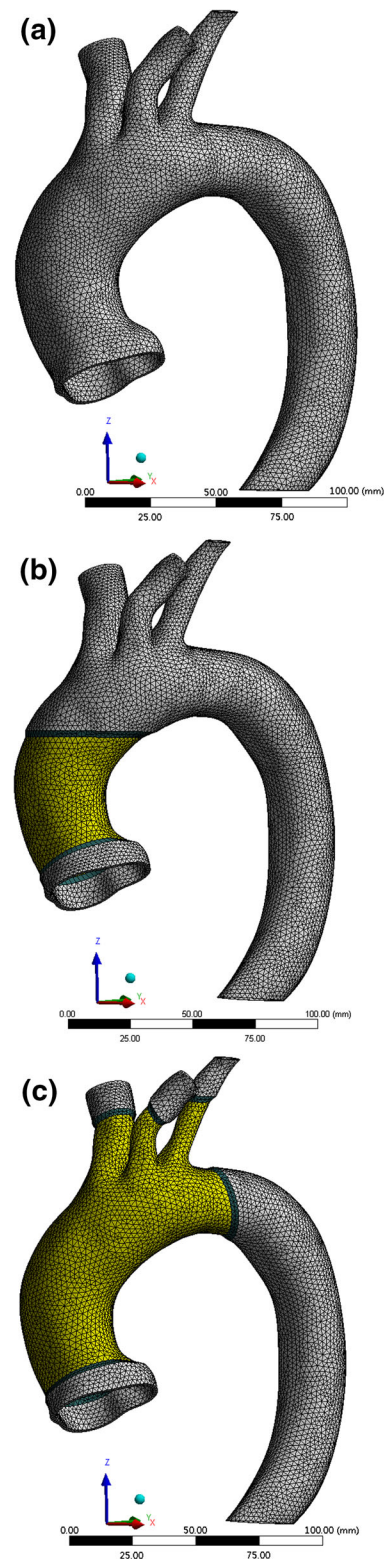
aortic arch with a high spatial resolution (<0.4 mm in all axes). Mesh independence was confirmed by increasing the number of elements in the mesh until the

peak stress obtained using the present mesh differed by less than 2% from that obtained using the previous mesh. The optimum mesh density thus obtained was approximately 1.0–1.5 million cells.

Tetrahedral elements were adopted to model the aortas and the vascular graft. Figure 5 presents the meshes typical of those used in the analysis. Three analyses were performed for each aortic arch—one for the arch with no graft (control); one for the arch after it has received HAR and one for the arch after it had received TAR. The von Mises stresses were thus compared.

Statistical Analysis

Descriptive statistics for categorical variables are presented as frequencies and percentages whereas continuous variables are expressed as mean (standard deviation) or median (range) as appropriate. Categorical variables for hemiarches and total arches were compared by performing the χ^2 test or Fisher exact test and continuous variables were compared using the 2-sample t test or Wilcoxon rank sum test as appropriate. All statistical tests were 2-sided with the alpha level set to 0.05 to identify statistical significance.

RESULTS

Mechanical Properties of Polyester Woven Graft

Figure 6 plots the measured stress–strain curves of the prepared samples that were obtained by cutting along the woven grafts in the axial and circumferential directions. The elastic moduli along the axial direction (E_x) and circumferential direction (E_y) were 6.3 and 72.7 MPa, respectively, while the Poisson's ratios were found to be 0.36 and 0.4, respectively. Owing to the
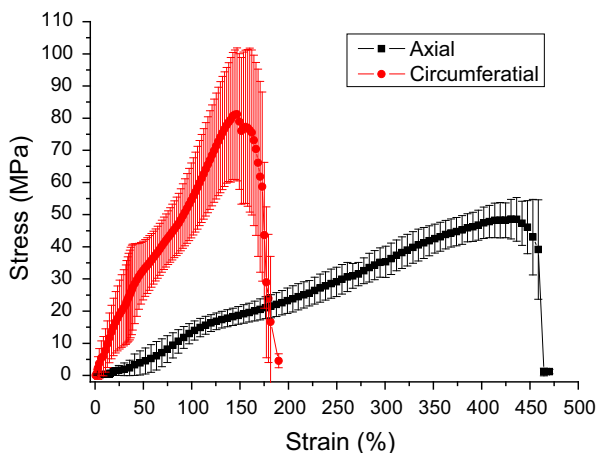
small thickness, the elastic modulus (E_z) and the Poisson's ratio (v_{zx}) in the thickness direction were assumed to be equal to those in the axial direction E_x and v_{xy} respectively. The shear moduli (G) were calculated using the following equations:

$$G_{xy} = \frac{E_x E_y}{E_x + E_y + 2v_{xy}E_x} \tag{1}$$

$$G_{yz} = \frac{E_y E_z}{E_y + E_z + 2v_{yz}E_y} \tag{2}$$

$$G_{xz} = \frac{E_x E_z}{E_x + E_z + 2v_{xz}E_x} \tag{3}$$

Table 1 lists the parameters of the vascular grafts that were used for the FEA.

Fluid Dynamic/Wall Stress Analysis

The flow patterns and the distribution of pressure imposed on the vessels by the blood in the 11 subjects were simulated using the finite element method. Figure 7 plots the calculated pressure distribution in the aortic arch in one of subjects, while Table 2 lists the maximum flow velocity, pressure and wall shear stress for the 11 subjects. The pressure distributions were used as the boundary conditions for the subsequent elastic stress analysis.

Table 3 presents the maximal aortic stress distribution in the control, HAR and TAR groups. Figure 8 shows the computed stress distribution along the midline in the coronal plane of three representative patients in the control group. The peak wall stress of the normal thoracic aorta (control group) was 0.91 ± 0.77 MPa (with a range of 0.39–3.05 MPa). The locations of maximal wall stress were at the sinotubular junction and in the area just distal to the orifices of supra-aortic vessels. Figures 9 and 10 display the computed stress distributions along the anastomosis lines of the HAR and the anastomosis line

FIGURE 6. Stress-strain curves of the vascular grafts.

TABLE 1. Parameters of vascular grafts used for FEM analysis.

Parameters	Value
E_x	6.3 MPa
E_y	72.7 MPa
E_z	6.3 MPa
v_{xy}	0.36
v_{yz}	0.4
v_{zx}	0.36
G_{xy}	3.5 MPa
G_{yz}	2.25 MPa
G_{xz}	5.5 MPa

of the TAR in the distal residual aorta in patients who had received HAR and TAR, respectively. For those subjects that had received HAR, the average peak wall stress was 0.55 ± 0.12 MPa (with a range of 0.36–0.71 MPa) at the proximal residual aorta, 0.88 ± 0.22 MPa (with a range of 0.52–1.20 MPa) at the proximal anastomosis, 0.75 ± 0.15 MPa (with a range of 0.56–1.05 MPa) at the distal anastomosis, and 0.90 ± 0.54 MPa (with a range of 0.46 to 2.24 MPa) at the distal residual aorta. The maximal wall stress at the distal anastomosis was observed in the left half of the anastomosis in five patients (45%) and in both the left and right halves in six patients. The location of maximal wall stress in the distal residual aorta was in the area just distal to the orifices of the supra-aortic vessels (Fig. 9).

The results in Table 3 suggest that the average peak wall stress in the thoracic aorta after TAR was 0.56 ± 0.14 MPa (with a range of 0.38–0.84 MPa) at the proximal residual aorta, 0.92 ± 0.25 MPa (with a range of 0.65–1.40 MPa) at the proximal anastomosis, 0.59 ± 0.18 MPa (with a range of 0.34–0.89 MPa) at the distal anastomosis, and 0.46 ± 0.25 MPa (with a range of 0.27–0.99 MPa) at the distal residual aorta. The maximal wall stress at the residual distal aorta was located at the proximal descending aorta just distal to the anastomosis (Fig. 10). When compared to the peak wall stress of the thoracic aorta after HAR, the peak wall stress of aorta following TAR was significantly lower at the distal residual aorta ($p = 0.02$).

DISCUSSION

Computational finite element analysis has become a powerful and valuable tool in research into the biomechanical behavior of the aorta with various aortic diseases.[2,11,12,14,17,23] Aortic aneurysm rupture is generally believed to occur when the aortic wall stress exceeds the yield strength. Venkatasubramaniam *et al.*[23] demonstrated that the peak wall stress,

10630 10637 10644 10651 10658 10665 10672 10679 10686 10693 10700
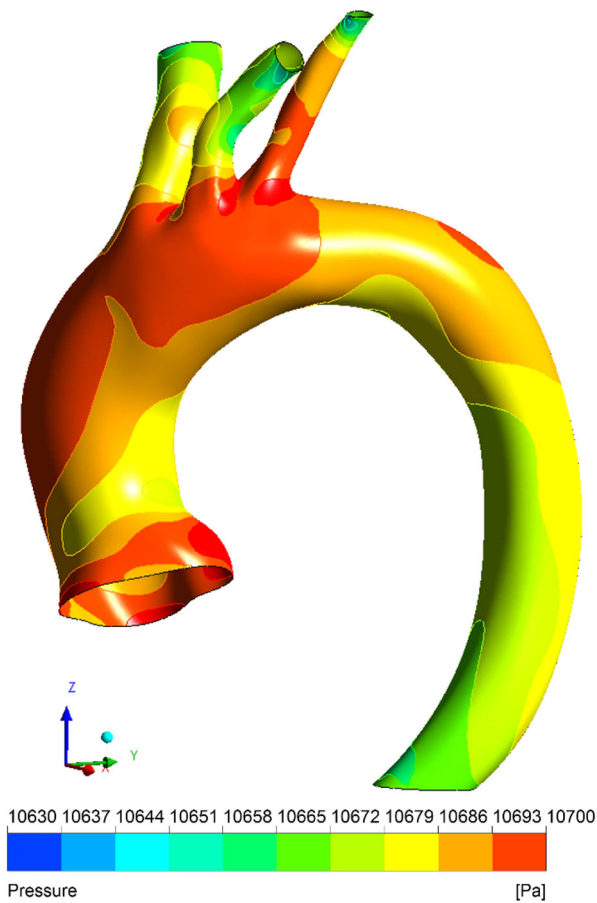
Pressure [Pa]

FIGURE 7. Representative calculated pressure distribution in aortas.

TABLE 2. Computed velocity and pressure of blood flow, and wall shear stress caused thereby.

	Velocity (m/s)		Pressure (Pa)		Wall shear stress (Pa)	
Patient no.	Max (Ascending aorta)	Min (Descending aorta)	Max (Arch branch)	Min (Ascending aorta)	Max (Ascending aorta)	Min (Arch bottom)
01	0.274	0.0126	10730	10650	0.799	0
02	0.3653	0.006304	10770	10650	1.259	0
03	0.3485	0.00117	10760	10640	0.908107	0
04	0.2632	0.004278	10720	10660	0.489	0
05	0.292	0.005413	10720	10640	0.611512	0
06	0.3313	0.0001716	10730	10630	0.7661	0
07	0.3267	0.009735	10720	10640	0.7697	0
08	0.2248	0.0005444	10700	10650	0.4005	0
09	0.2388	0.004257	10690	10650	0.308	0
10	0.3299	0.002628	10730	10650	0.756	0
11	0.2641	0.003844	10700	10650	0.4495	0
Mean	0.29624	0.00463	10724.55	10646.36	0.68331	0
SD	0.04672	0.00383	24.23371	8.0904	0.27081	0

TABLE 3. Computed maximal stress distribution in control, hemiarch replacement and total arch replacement groups.

Maximal stress (MPa)	Control	Hemiarch replacement					Total arch replacement						
	Aorta	Proximal residual aorta	Proximal anastomosis	Graft	Distal anastomosis	Distal residual aorta	Proximal residual aorta	Proximal anastomosis	Graft	Arch branch anastomoses	Arch branches	Distal anastomosis	Distal residual aorta
1	0.89626	0.42155	0.79237	5.1978	0.82966	0.91823	0.41492	0.76858	11.258	0.33546	0.22614	0.41223	0.31714
2	1.1682	0.57756	1.10640	3.4088	0.82498	1.3399	0.55492	1.1804	6.9935	0.35837	0.19334	0.7628	0.39429
3	0.41829	0.43539	0.78120	2.9423	0.59118	0.45789	0.43985	0.77997	3.2375	0.35874	0.21218	0.34483	0.27225
4	0.38738	0.35948	0.51860	3.5903	0.61037	0.45948	0.38351	0.65247	4.7243	0.2741	0.16372	0.89493	0.49682
5	0.96208	0.51147	0.68488	4.1485	0.74294	0.9721	0.53542	0.72328	11.809	0.45549	0.38924	0.68462	0.38924
6	1.06910	0.69410	1.03210	6.5009	0.79491	1.1775	0.6619	0.95112	9.0287	0.69371	0.33854	0.76419	0.89449
7	0.39887	0.71081	1.19870	3.9395	1.0532	0.46498	0.83619	1.3987	4.1466	0.37613	0.16726	0.45997	0.34923
8	3.05130	0.58550	0.76438	4.0693	0.84929	2.2429	0.55526	0.67672	10.926	1.2106	0.64617	0.71768	0.98614
9	0.40995	0.69388	0.87987	4.6563	0.75456	0.50915	0.72628	0.94374	4.7071	0.36695	0.11356	0.43588	0.27885
10	0.53898	0.49324	0.76198	4.7223	0.56492	0.60266	0.52228	0.85788	4.4752	0.48152	0.29182	0.4527	0.40829
11	0.73794	0.52700	1.19160	3.88	0.59854	0.75288	0.51711	1.22	6.3821	0.38402	0.15731	0.54568	0.31262
Mean	0.91258	0.54636	0.88292	4.27782	0.74678	0.89979	0.55888	0.92299	7.06255	0.48137	0.26357	0.58868	0.46358
SD	0.76638	0.11848	0.22054	0.97333	0.14753	0.54046	0.13596	0.24581	3.16598	0.26563	0.04579	0.1821	0.24521
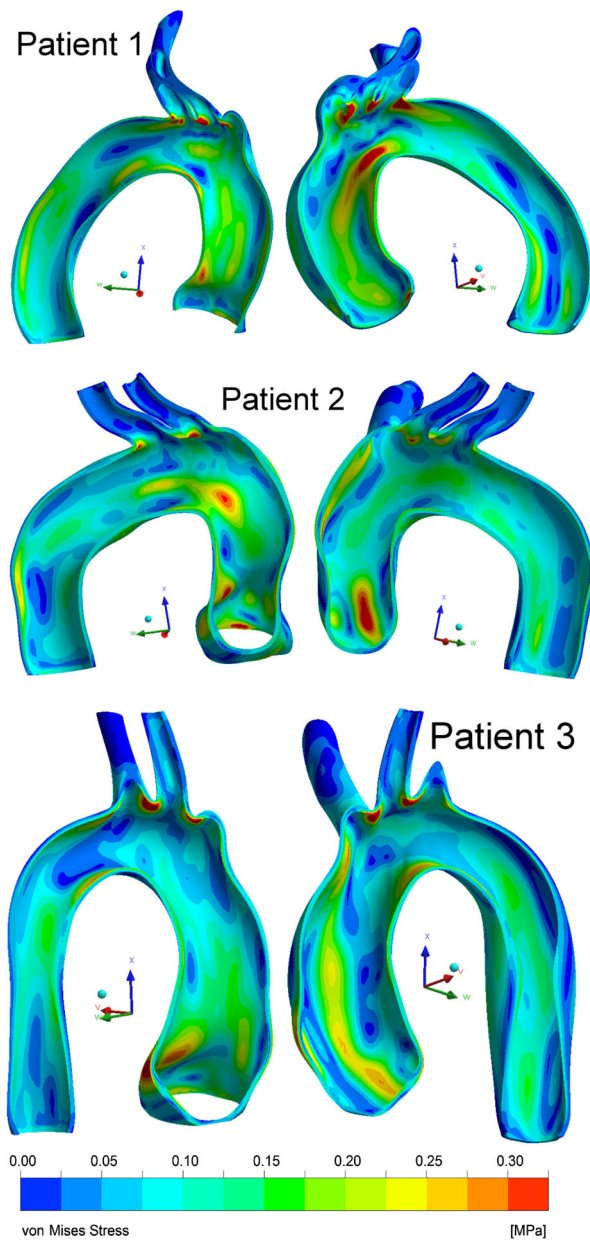
FIGURE 8. Stress distribution in control group (unit: MPa).

FIGURE 9. Stress distribution in distal residual aorta in patients who had received hemiarch replacement (unit: MPa).

calculated from CT images and by finite element analysis, was significantly higher in a ruptured abdominal aortic aneurysm (AAA) than in a non-ruptured aneurysm. In patients with an identifiable site of rupture on the CT scan, the area of peak wall stress was correlated with the rupture site. Nathan *et al.*[14] found increased wall stress in the thoracic aorta above the sinotubular junction and distal to the left subclavian artery, where tears in the primary intima typically result in type A and type B aortic dissections. Shang *et al.*[17] found that the computational peak wall stress in thoracic aortic aneurysms was more strongly correla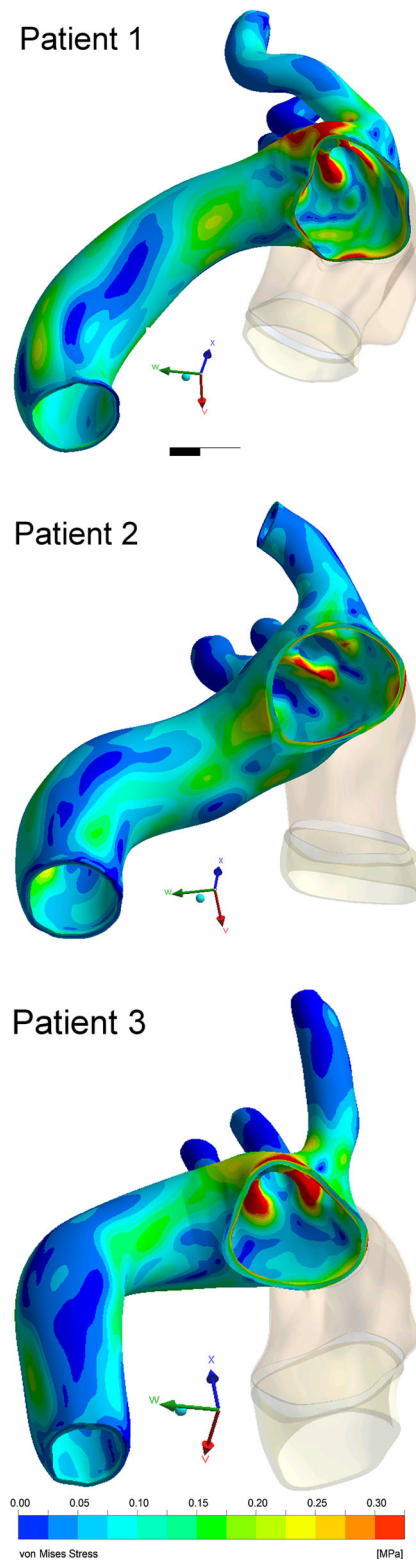ted with the aneurysm expansion rate than with the maximal aortic diameter. Aneurysms that required surgical intervention exhibited significantly higher peak wall stresses than those did not.

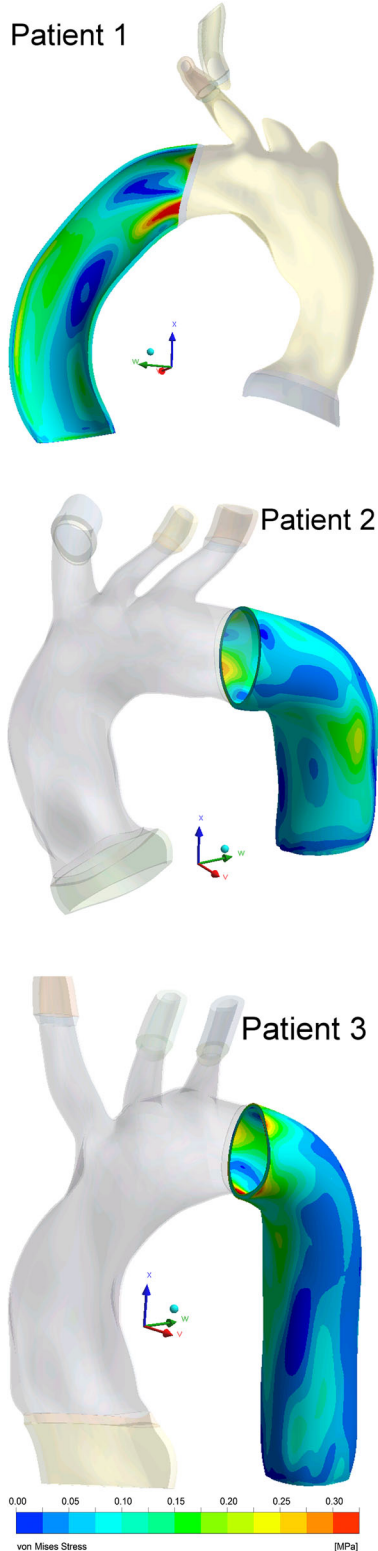This study represents one of the first biomechanical investigations to compare two surgical approaches for replacing the aortic arch. FEA was used therein to demonstrate that HAR was associated with a higher peak wall stress at the residual distal aorta than was TAR. HAR was also associated with a higher peak stress at the distal anastomosis although statistical significance was not reached ($p = 0.08$). The location of the peak wall stress at the distal residual aorta was just distal to the orifices of the supra-aortic vessels after HAR and at the proximal descending aorta just distal to the anastomosis after TAR. Regions of higher stress are more prone to disease. The locations of peak wall stress in the residual distal aorta are consistent with the locations where aortic aneurysms tend to develop after operations for type A aortic dissections.

An extended arch replacement for acute type A aortic dissection reduces the incidence of a patent false lumen and the need for reoperation below those achieved using a more limited ascending aortic or hemiarch replacement.[8,10,20–22] We speculate that in these two procedures, HAR and TAR, the aortic arch is replaced to different extents using a woven polyester graft, and their different mechanical properties may contribute to the different results. In this study, the peak wall stress at the distal residual aorta was significantly higher after HAR than after TAR. We also noted a trend toward higher peak wall stress at the distal anastomosis after HAR, although not a statistically significant one ($p = 0.08$). The increased stress at the distal anastomosis may introduce new breaks in the fragile intima tissue, resulting in a persistent patent

FIGURE 10. Stress distribution in distal residual aorta in patients who had received total arch replacement (unit: MPa).

FIGURE 11. Intima break in distal aortic anastomosis (arrow) in a patient who underwent hemiarch replacement for type A aortic dissection.

false lumen (Fig. 11). The increase in stress at the distal residual aorta may contribute to the development of subsequent thoracic aortic aneurysm and thereby increase the risk of re-operation.

This study presents a good example of the use of FEM to analyze stress in HAR and TAR. The results of the analysis provide insights into the behavior of the aortic replacement and related mechanical stress that are associated with potential aneurysm rupture. These findings suggest that HAR leads to a higher peak stress at the distal aortic anastomosis than does TAR (although not to a statistically significant extent) and at the distal residual aorta, potentially causing rupture at the anastomosis sites and increasing the risk of subsequent aneurysm formation. The simulation in this study may provide an improved understanding of the influence of various surgical procedures for graft replacement on the formation of induced stresses in the aorta. Numerical simulation of the arch replacement can be used to guide corrective measures if the problem arises, and also prevent a potential problem from occurring in the first place.

LIMITATIONS

Although this study provides a theoretical basis for calculating mechanical stress in an aortic arch following different surgical methods for aortic arch replacement, it has some limitations. First, the thickness of the walls of arteries was assumed to be constant within and among patients. Future studies should consider patient-specific arterial wall thickness with regional variations thereof. Second, the physical characteristics of the arterial-wall, which were parameters that were input to the FEA model, were obtained from published data, and these characteristics may differ for diseased arteries. Specifically, diseased arteries that undergo greater dilation exhibit much greater surface-contact stresses. Third, the use of isotropic, linear, elastic tetrahedral elements in the FEA represents a simplification. A more realistic non-linear model should be used to capture the properties of the vessels more accurately. Fourth, the mechanical properties of the aortic graft were tested under dry conditions, and the properties of an aortic graft in contact with blood may be different. All of these issues will be addressed in the authors' future research.

CONCLUSIONS

In this study, FEA was used to examine the deformation and stress distribution in HAR and TAR using a hybrid fluid–structure interaction analysis that combines computational fluid dynamics with structural static analysis. Geometric information concerning the aortas of 11 subjects was obtained from contrast-enhanced CT scan data. CT images were imported into medical image processing software to construct 3D models of the aortas. The stress distribution of the aortas and the grafts that had received HAR or TAR were analyzed. Numerical results demonstrated that the aortas following TAR exhibited lower stress than those following HAR. Higher stresses are more likely to cause arterial wall injury and are associated with an increased risk of rupture. The finite element analysis of the aortas and the aortic grafts herein provides useful information for physicians to help them better understand the problems that may arise after various surgical procedures.

DISCLOSURE

The authors report no conflicts of interest with respect to this work.

REFERENCES

[1]Azadani, A. N., S. Chitsaz, P. B. Matthews, N. Jaussaud, J. Leung, T. Tsinman, L. Ge, and E. E. Tseng. Comparison of mechanical properties of human ascending aorta and aortic sinuses. *Ann. Thorac. Surg.* 93:87–94, 2012.
[2]Beller, C. J., M. R. Labrosse, M. J. Thubrikar, and F. Robicsek. Role of aortic root motion in the pathogenesis of aortic dissection. *Circulation* 109:763–769, 2004.
[3]Beller, C. J., M. R. Labrosse, M. J. Thubrikar, G. Szabo, F. Robicsek, and S. Hagl. Increased aortic wall stress in aortic insufficiency: clinical data and computer model. *Eur. J. Cardiothorac. Surg.* 27:270–275, 2005.
[4]Dur, O., C. G. DeGroff, B. B. Keller, and K. Pekkan. Optimization of inflow waveform phase-difference for minimized total cavopulmonary power loss. *J. Biomech. Eng.* 132:031012, 2010.
[5]Dur, O., S. T. Coskun, K. O. Coskun, D. Frakes, B. L. Kara, and K. Pekkan. Computer aided patient specific coronary artery graft design improvements using CFD coupled shape optimizer. Cardiovasc. *Eng. Technol.* 2:35–47, 2011.
[6]Fukui, T., T. Matsumoto, T. Tanaka, T. Ohashi, K. Kumagai, H. Akimoto, K. Tabayashi, and M. Sato. *In vivo* mechanical properties of thoracic aneurysmal wall estimated from *in vitro* biaxial tensile test. *Biomed. Mater. Eng.* 15:295–305, 2005.

[7]Fung, Y. C., and S. Q. Liu. Determination of the mechanical properties of the different layers of blood vessels *in vivo*. *Proc. Natl. Acad. Sci. USA*. 92:2169–2173, 1995.

[8]Hirotani, T., T. Nakamichi, M. Munakata, and S. Takeuchi. Routine extended graft replacement for an acute type A aortic dissection and the patency of the residual false channel. *Ann. Thorac. Surg.* 76:1957–1961, 2003.

[9]Jeltsch, M., O. Klass, S. Klein, S. Feuerlein, A. J. Aschoff, H. J. Brambs, and M. H. Hoffmann. Aortic wall thickness assessed by multidetector computed tomography as a predictor of coronary atherosclerosis. *Int. J. Cardiovasc. Imaging* 25:209–217, 2009.

[10]Kazui, T., K. Yamashita, N. Washiyama, H. Terada, A. H. Bashar, T. Suzuki, and K. Ohkura. Impact of an aggressive surgical approach on surgical outcome in type A aortic dissection. *Ann. Thorac. Surg.* 74:S1844–S1847, 2002.

[11]Labrosse, M. R., C. J. Beller, T. Mesana, and J. P. Veinot. Mechanical behavior of human aortas: experiments, material constants and 3-D finite element modeling including residual stress. *J. Biomech.* 42:996–1004, 2009.

[12]Larsson, E., F. Labruto, T. C. Gasser, J. Swedenborg, and R. Hultgren. Analysis of aortic wall stress and rupture risk in patients with abdominal aortic aneurysm with a gender perspective. *J. Vasc. Surg.* 54:295–299, 2011.

[13]Minakawa, M., I. Fukuda, J. Yamazaki, K. Fukui, H. Yanaoka, and T. Inamura. Effect of cannula shape on aortic wall and flow turbulence: hydrodynamic study during extracorporeal circulation in mock thoracic aorta. *Artif. Organs* 31:880–886, 2007.

[14]Nathan, D. P., C. Xu, J. H. Gorman, 3rd, R. M. Fairman, J. E. Bavaria, R. C. Gorman, K. B. Chandran, and B. M. Jackson. Pathogenesis of acute aortic dissection: a finite element stress analysis. *Ann. Thorac. Surg.* 91:458–464, 2011.

[15]Pekkan, K., O. Dur, K. Sundareswaran, K. Kanter, M. Fogel, A. Yoganathan, and A. Undar. Neonatal aortic arch hemodynamics and perfusion during cardiopulmonary bypass. *J. Biomech. Eng.* 130:061012, 2008.

[16]Shahcheraghi, N., H. A. Dwyer, A. Y. Cheer, A. I. Barakat, and T. Rutaganira. Unsteady and three-dimensional simulation of blood flow in the human aortic arch. *J. Biomech. Eng.* 124:378–387, 2002.

[17]Shang, E. K., D. P. Nathan, S. R. Sprinkle, S. C. Vigmostad, R. M. Fairman, J. E. Bavaria, R. C. Gorman, J. H. Gorman, 3rd, K. B. Chandran, and B. M. Jackson. Peak wall stress predicts expansion rate in descending thoracic aortic aneurysms. *Ann. Thorac. Surg.* 95:593–598, 2013.

[18]Speelman, L., E. M. H. Bosboom, G. W. Schurink, F. A. Hellenthal, J. Buth, M. Breeuwer, M. J. Jacobs, and F. N. van de Vosse. Patient-specific AAA wall stress analysis: 99-percentile vs. peak stress. *Eur. J. Vasc. Endovasc. Surg.* 36:668–676, 2008.

[19]Sundareswaran, K. S., K. Pekkan, L. P. Dasi, K. Whitehead, S. Sharma, K. R. Kanter, M. A. Fogel, and A. P. Yoganathan. The total cavopulmonary connection resistance: a significant impact on single ventricle hemodynamics at rest and exercise. *Am. J. Physiol. Heart Circ. Physiol.* 295:H2427–H2435, 2008.

[20]Takahara, Y., Y. Sudo, K. Mogi, M. Nakayama, and M. Sakurai. Total aortic arch grafting for acute type A dissection: analysis of residual false lumen. *Ann. Thorac. Surg.* 73:450–454, 2002.

[21]Tan, M. E., K. M. Dossche, W. J. Morshuis, J. C. Kelder, F. G. Waanders, and M. A. Schepens. Is extended arch replacement for acute type A aortic dissection an additional risk factor for mortality? *Ann. Thorac. Surg.* 76:1209–1214, 2003.

[22]Urbanski, P. P., A. Siebel, M. Zacher, and R. W. Hacker. Is extended aortic replacement in acute type A dissection justifiable? *Ann. Thorac. Surg.* 75:525–529, 2003.

[23]Venkatasubramaniam, A. K., M. J. Fagan, T. Mehta, K. J. Mylankal, B. Ray, G. Kuhan, I. C. Chetter, and P. T. McCollum. A comparative study of aortic wall stress using finite element analysis for ruptured and non-ruptured abdominal aortic aneurysms. *Eur. J. Vasc. Endovasc. Surg.* 28:168–176, 2004.